Photophysics of 9,9-dimethylacridan substituted phenylstyrylpyrimidines exhibiting long lived intramolecular charge transfer fluorescence and aggregation induced emission characteristics

Michaela Fecková, Ioannis Konstantinos Kalis, Thierry Roisnel, Pascal Le Poul, Oldřich Pytela, Milan Klikar, Françoise Robin Le Guen, Filip Bureš, Mihalis Fakis, Sylvain Achelle

10.1002/chem.202004328

Photophysics of 9,9-dimethylacridan substituted phenylstyrylpyrimidines exhibiting long lived intramolecular charge transfer fluorescence and aggregation induced emission characteristics

Michaela Fecková,[a,b] Ioannis Konstantinos Kalis[c], Thierry Roisnel,[a] Pascal le Poul,[a] Oldřich Pytela,[b] Milan Klikar,[b] Françoise Robin-le Guen,[a] Filip Bureš,[b,*] Mihalis Fakis,[c,*] Sylvain Achelle[a,*]

[a] Univ. Rennes, CNRS, Institut des Sciences Chimique de Rennes – UMR 6226, F 35000 Rennes, France E-mail : sylvain.achelle@univ-rennes1.fr

[b] Institute of Organic Chemistry and Technology, Faculty of Chemical Technology, University of Pardubice, Studenská 573, CZ-53210 Pardubice, Czech Republic E-mail : filip.bures@upce.cz

[c] Department of Physics, University of Patras, GR-26504 Patras, Greece E-mail: fakis@upatras.gr

TOC

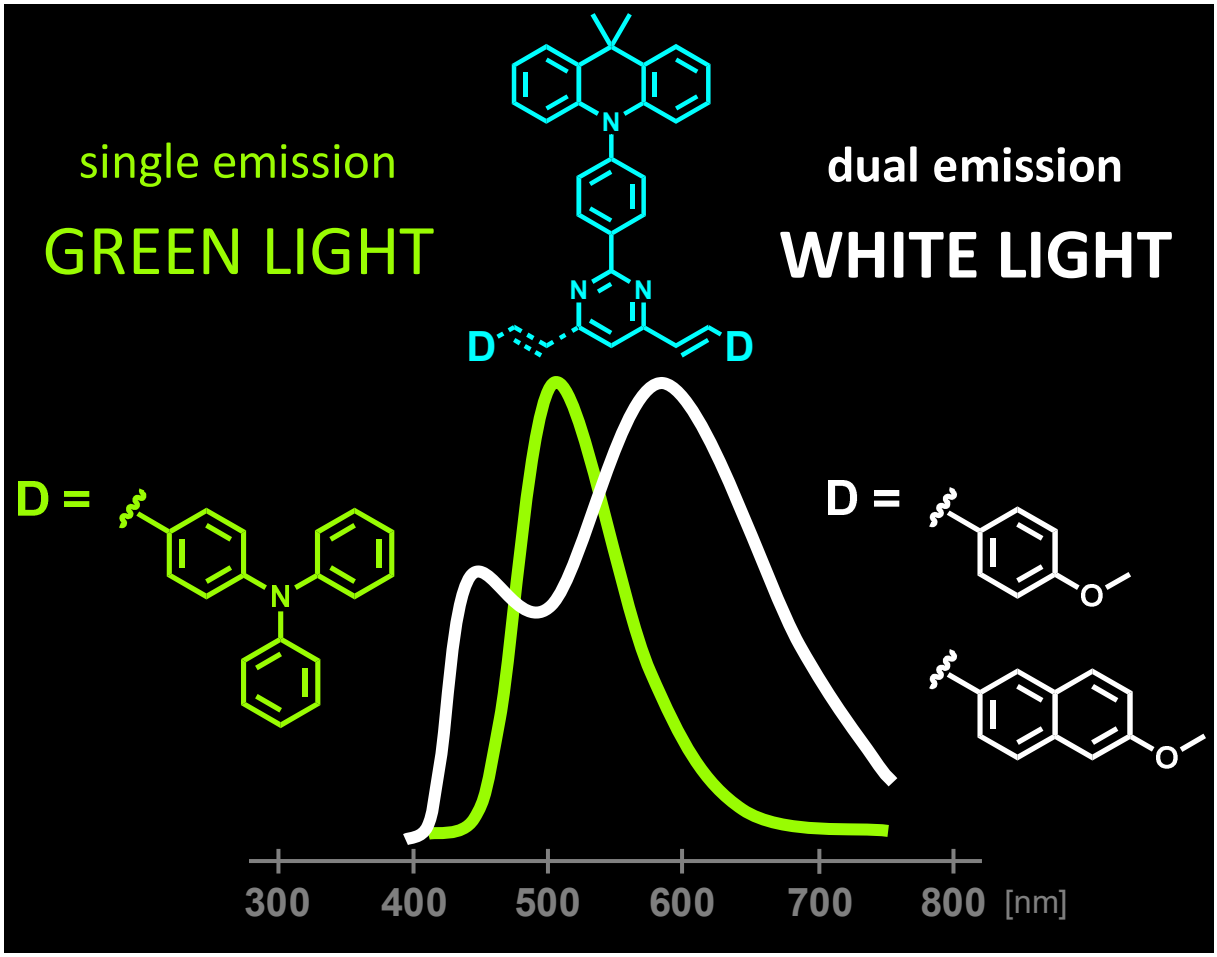

10.1002/chem.202004328

Abstract

Six pyrimidine-based push-pull systems substituted at positions C2 and C4/6 with phenylacridan and styryl moieties, employing methoxy or *N*,*N*-diphenylamino donors, have been designed and synthesized involving cross-coupling and Knoevenagel reactions. X-ray analysis confirmed their molecular structure featuring the acridan moiety arranged perpendicularly to the residual π-system. Photophysical studies revealed significant differences between the methoxy and *N,N*-diphenylamno chromophores. Solvatochromic studies revealed that the methoxy derivatives show dual emission in polar solvents. Time resolved spectroscopy revealed that the higher energy band involves very fast (<80 ps) prompt fluorescence while the lower energy one includes long components (~30 ns) due to long lived ICT fluorescence. In contrast to *N*,*N*-diphenylamino chromophores, the methoxy derivatives also showed aggregation induced emission in THF/water mixtures as well as dual emission in thin films, covering almost the whole visible spectrum with corresponding chromaticity coordinates being not far from pure white light. These properties render the methoxy derivatives as very promising organic materials for WOLEDs.

Keywords: Pyrimidine, Dual emission, Intramolecular charge transfer, Aggregation induced emission,

Introduction

During the past few years, there has been a great interest in the design of organic emissive molecules that are indeed the key element of organic light emitting diodes (OLEDs).[1] Both fluorescent and phosphorescent emitters were utilized in the first and second generation OLEDs.[2] Whereas the first generation OLEDs suffer from an internal quantum efficiency (IQE) limited to 25% (the external quantum efficiency (EQE) is often below 5%),[3] the second generation OLEDs (so-called PhOLEDs) overcome this problem and IQE can reach

theoretically 100 %. However, materials for PhOLEDs are mostly based on heavy metal (Ir, Pt, Os…) complexes, which are rather expensive, have limited resources, and exhibit potential toxicity.[4] Thermally activated delayed fluorescence (TADF) is another recently utilized approach towards third generation OLEDs with theoretical IQE of 100% and the real EQE up to 30%.[2,5] This principle utilizes conversion of triplet excitons into luminescent singlet excitons via a reverse intersystem crossing (RISC) leading to increased fluorescent lifetime (up to several microseconds).[2,5] In principle, a TADF emitter should possess a small energy difference between T_1 and S_1 excited states (ΔE_{ST}),[6] which is generally achieved by orthogonal arrangement of the S_1 state with spatially separated HOMO and LUMO.[5a,5b,7] In this context, bulky electron-donating substituents such as carbazol-9-yl,[8] acridan,[9] spiroacridan,[10] phenoxazine[11] and azasiline,[12] with a phenylene linker have been often used.

Dual emission is generally obtained by a combination of luminophores that are linked together.[13] Two emission bands can be also observed in case of coexistence of two forms of the same compound (equilibrium). This is for example what is observed with excimer/exciplex[14] or when excited state intramolecular proton transfer occurs.[15] Recently, single-luminophore presenting dual emission based on localized and charge-transfer excited states or two charge-transfer excited states have been described.[16]

Apart from the aforementioned properties, organic chromophores applicable for OLEDs should be also highly emissive in the solid state. However, many push-pull chromophores that are highly luminescent in solution, exhibit aggregation-caused quenching (ACQ) and are therefore non (or weakly) emissive in solid state.[17] Nevertheless, in specific cases, aggregation induced emission (AIE), a concept proposed by Tang et al in 2001, induces intensive emission in the solid state of non (or slightly) emissive chromophores in solution.[18] In general, a reduction of π-π stacking and a restriction of intramolecular motions have been

recognized as the working mechanisms of AIE. In order to reduce the π-π stacking, molecules suitable for AIE are not planar but adopt a twisted conformation. When both AIE and TADF phenomena are combined, the term of aggregation-induced delayed fluorescence (AIDF) is used.[19]

Among numerous series of emitters, push-pull pyrimidine chromophores are well-known for their luminescence properties.[20] In particular, some of us have described a large library of styrylpyrimidine fluorophores[21] and it is also noteworthy that pyrimidine seems to exhibit all necessary properties towards applications in lighting devices. The pyrimidine ring can be protonated and in specific cases white light emission can be obtained from a mixture of neutral and protonated forms by controlling the amount of the used acid.[22] Also, the pyrimidine core has been used in the structure of TADF chromophores leading to highly efficient blue OLEDs with EQE > 25%.[23] Compared to the widely used triazine, the pyrimidine core is a weaker electron-withdrawing group, and therefore pyrimidine derivatives exhibit increased band gap energy (E_g) and higher S_1 and T_1 energy levels.[24] Finally, AIE was also reported for some 4,6-distyrylpyrimidimine derivatives.[25]

Based on the possible matching of the aforementioned OLED requirements and pyrimidine fundamental characteristics, we have designed a series of 4-styryl and 4,6-distyrylpyrimidine chromophores that are linked to an acridan fragment via a phenylene linker in position C2 of the pyrimidine core. In these molecules we aim to combine the AIE properties together with the Intramolecular Charge Transfer (ICT) fluorescence. Their synthesis, photophysical properties, some X-ray structures and quantum-chemical investigations are reported herein. In principle, the charge transfer may occur either from the phenylacridan C2 branch or the C4/C6 styryl branches which are substituted either by methoxy or *N,N*-diphenylamino electron donors. In case of methoxy substituted styryl branches, this arrangement leads to dual emission with long-lived fluorescence characteristics.

The AIE is also reported in solutions upon addition of a non-solvent together with broad white light dual emission in neat films rendering the herein reported chromophores potentially suitable for application as single emissive layers in WOLEDs.

Results and Discussion

Synthesis

Compounds in the series **3** and **4** were obtained in two steps from commercially available 2-chloro-4-methylpyrimidine and 2-chloro-4,6-dimethylpyrimidine respectively (Scheme 1). In both cases, the first step consists of a palladium catalyzed Suzuki-Miyaura cross coupling reaction with 4-(9,9-dimethyl-9,10-dihydroacridine)phenylboronic acid pinacol ester leading to intermediates **1** and **2** with moderate yields. As well documented in the chemistry of pyrimidine, the electron-withdrawing character of the pyrimidinyl fragment permits the oxidative addition of palladium into the chlorine-carbon bond without the use of special and expensive ligands.[26] The second step involves Knoevenagel condensations with the corresponding aldehyde in boiling aqueous sodium hydroxide in the presence of Aliquat 336 phase transfer catalyst, according to the conditions initially described by Vanden Eynde[27] and developed by us.[21a-c] It should be noted that the isolated yields of *N*,*N*-diphenylamino derivatives **c** are significantly lower than those of the methoxy ones (**a** and **b**) due to complicated purification. All compounds were fully characterized by ^{1}H and ^{13}C NMR (Figures S29-S44), as well as HRMS. According to previous observations,[21a-c] the condensation reactions generate only the *E*-isomer, as shown by the coupling constant of the ^{1}H NMR spectra ($J \approx 16$ Hz).

10.1002/chem.202004328

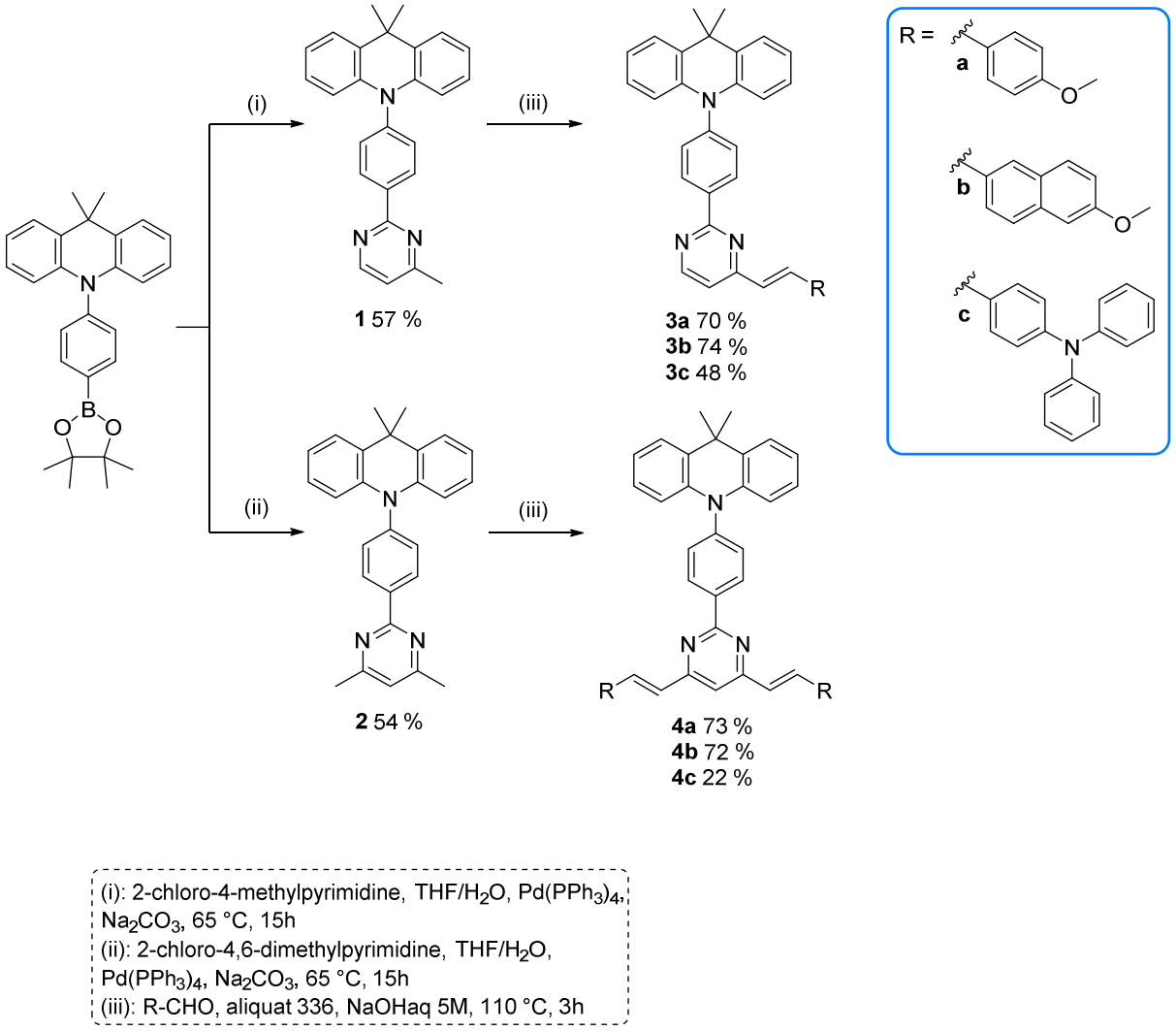

Scheme 1: Synthesis of the compounds in series **3** and **4**.

Thermal properties

The thermal stability of organic chromophores for potential application in OLEDs is a key parameter. Therefore, the thermal behavior of all target fluorophores **3**–**4** was examined by differential scanning calorimetry (DSC). Figure 1 shows thermograms of representative compounds **3a**–**c** while Table 1 lists the measured melting points (T_m) and temperatures of thermal decompositions (T_d). All DSC records are provided in the SI. The measured melting points and temperature of decomposition range from 199–271 and 370–380 °C, respectively. The compound **3c** was obtained as amorphous solid, this phenomenon is clearly reflected in its different thermal behavior. It follows, that the molecule **3c** does not melt but it undergoes a

10.1002/chem.202004328

glass transition at 70 °C. On the other hand, the other compounds **3a**,**b** and **4a–c** are crystalline solids, which sharply melted and their liquid phase proved to be stable during heating process up to ca. 375 °C. Upon continued heating, all target fluorophores **3–4** were gradually decomposed (T_d exceeded T_m by about ca. 110–175 °C). Moreover, the branched compound **4b** underwent monotropic solid-solid transition of its metastable crystals at 253 °C. Similarly, polymorphous enantiotropic transition was detected for compound **4a** between 140 and 150 °C. Based on the performed DSC analysis the following outcomes can be deduced:

- Within **4a–c**, the melting points are affected by the nature of peripheral methoxy or *N*,*N*-diphenylamino groups.
- Thermal decomposition of all compounds **3–4** does not depend on the peripheral donor (**a-c**) or branching (**3** or **4**). This is clearly demonstrated by almost identical T_d values for **3–4** (Fig. 1, Table 1).
- Their large thermal robustness is rather given by the parent acridan-pyrimidine scaffold. Variation of the peripheral groups or structural branching influences the thermal stability only negligibly.

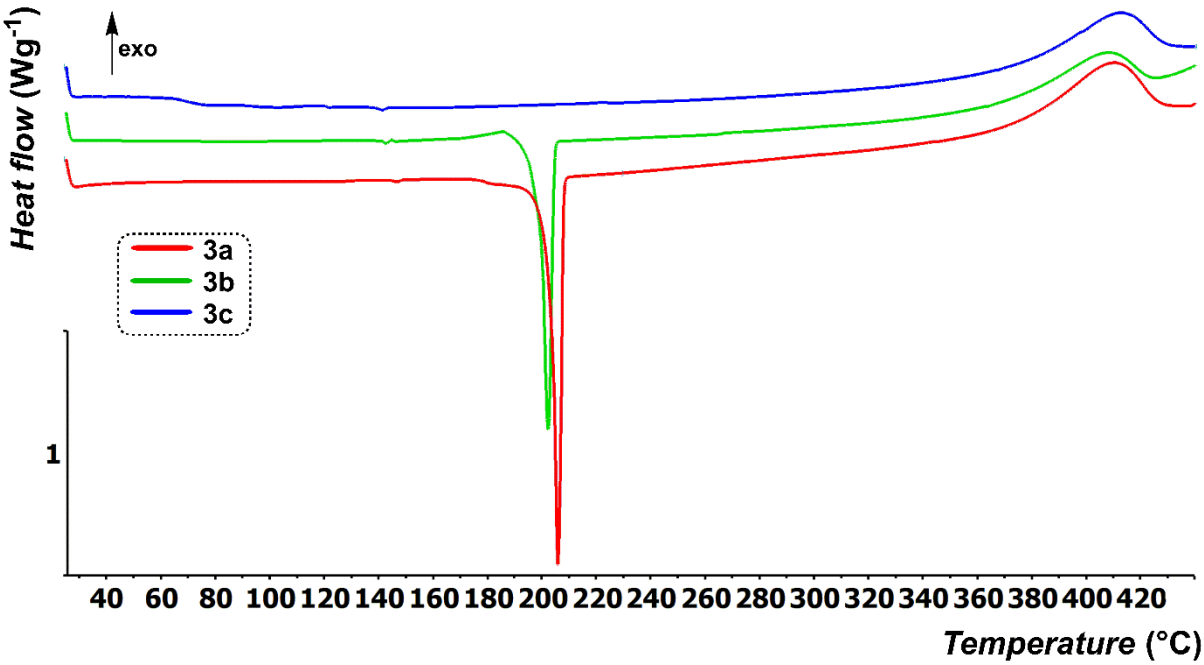

Figure 1. Representative DSC curves of compounds **3a-c** determined with a scanning rate of 3 °C/min under N_2 atmosphere.

10.1002/chem.202004328

Table 1. Thermal properties of **3**-**4**.

Comp.	T_m[a] (°C)	T_d[b] (°C)
3a	204	380
3b	199	375
3c	/	375
4a	201	370
4b	271	380
4c	233	380

[a] T_m = melting point (the point of intersection of a baseline and a tangent of thermal effect = onset).
[b] T_d = thermal decomposition (pyrolysis in N_2 atmosphere).

X-ray analysis

Crystals of **3a**, **4a** and **4c**, suitable for x-ray analysis, have been obtained by slow evaporation of their CH_2Cl_2/AcOEt solution. In all cases, the measured crystals, colorless or yellow prisms, confirm the proposed molecular structure, including the *E* stereoisomery of the alkene fragments (Figures 2 and S8, Tables S1-S3). For **3a** and **4a** a monoclinic crystal system is observed with a $P2_1/c$ space group whereas a triclinic crystal system with P1 space group has been identified for **4c**. In the case of **4a**, the presence of a molecule of ethyl acetate in the asymmetric unit of two molecules of **4a** has been observed (see Figure S7 in the ESI). In all cases, the dihedral angle between the pyrimidine core and the C2-phenyl fragment is below 17.5°, similar to those observed for other 2-phenylpyrimidine derivatives.[26] The RTG analyses of **3a**, **4a** and **4c** revealed a pre-twisted molecular structure with the vertical torsion angles between the acridan donor and the phenyl bridge of 82.3°, 81.1° and 85.0°. The torsion angles between the central pyrimidine core and the acridan fragment are 87.6, 88.3° and 83.3°, respectively. This structural arrangement would point to an important spatial separation of the frontier molecular orbitals, one of the necessary aspects to afford small ΔE_{ST} values. In contrast to previous styrylpyrimidines, the crystal structures further show that planes of the

10.1002/chem.202004328

phenyl rings of the styryl arms and the pyrimidine core are not coplanar (torsions angle < 22°).[21c,22c,28] For compounds **3a** and **4a**, bond length alternation (BLA) values of the vinylic linker were calculated to range between 0.1265 to 0.1316 Å. For **4c**, a significantly lower BLA value of 0.107 Å has been calculated for one of the two styryl branches. This would suggest a stronger charge transfer in one of the styryl arms for *N*,*N*-diphenylamino derivative **4c** than for methoxy derivatives **3a** and **4a**.

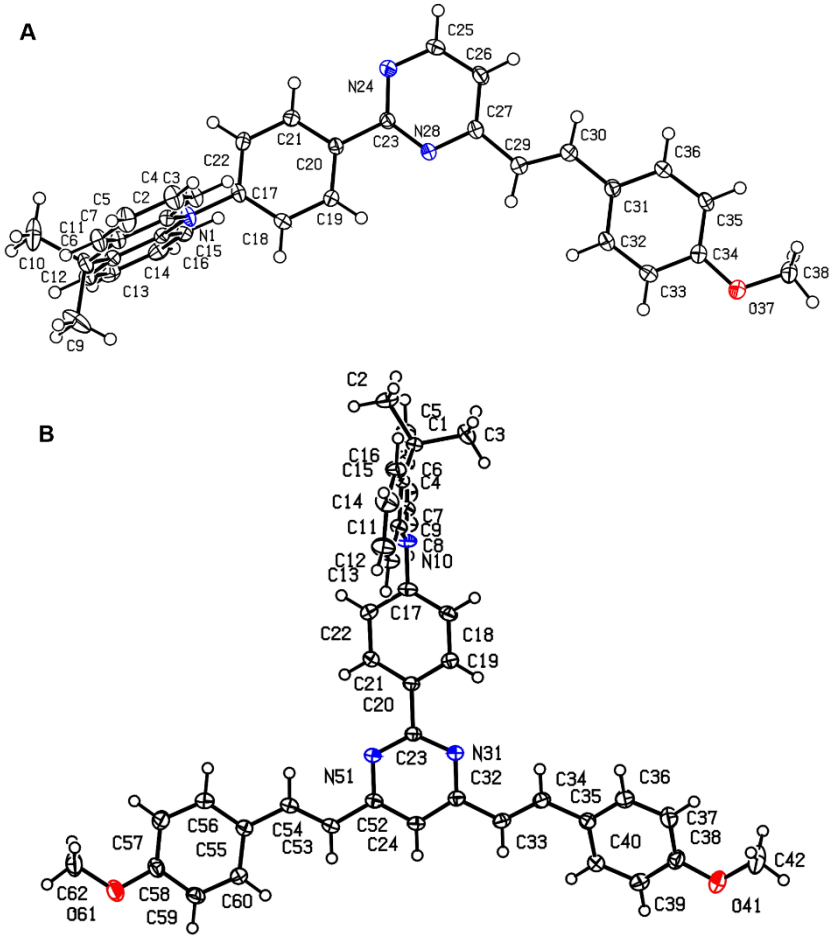

Figure 2: ORTEP drawings of chromophore **3a** (A) and **4a** (B) obtained at 150 K (R = 0.05). Thermal ellipsoids are shown at 50% probability level.

Density functional theory calculations

The spatial and electronic properties of the target chromophores were investigated using Gaussian®16W software[29] package at the DFT level. Initial geometries of molecules **3a-c**

10.1002/chem.202004328

and **4a**-**c** as well as the energies of their frontier molecular orbitals and ground state dipole moments μ were calculated at DFT B3LYP/6-311++G(3d,f,2p) level in vacuum. Theoretical electronic absorption spectra were calculated at TD-DFT (nstates = 8) level employing B3LYP/6-311++G(3d,f,2p) and CAM-B3LYP/6-311++G(2d,p). The calculated data are gathered in Table 2.

Table 2: DFT-calculated fundamental parameters of **3** and **4**.

Compd	E_{HOMO-1} (eV)[a]	E_{HOMO} (eV)[a]	E_{LUMO} (eV)[a]	E_{LUMO+1} (eV)[a]	ΔE (eV)[b]	μ (D)[a]	λ_{max}^{DFT} (nm(eV))[c]	GoS[d]
3a	–5.98	–5.10	–2.35	–1.75	2.75/3.63	7.1	352(3.52)/329(3.77)	C_s
3b	–5.89	–5.06	–2.45	–1.67	2.61/3.44	7.8	381(3.25)/337(3.68)	C_s
3c	–5.48	–5.08	–2.31	–1.67	2.77/3.17	6.5	434(2.86)/360(3.44)	None
4a	–5.87	–5.13	–2.42	–1.69	2.71/3.45	3.3	393(3.16)/343(3.62)	C_{2v}
4b	–5.66	–5.10	–2.46	–1.77	2.64/3.20	3.0	433(2.86)/359(3.45)	C_{2v}
4c	–5.31	–5.16	–2.36	–1.72	2.80/2.95	5.3	474(2.62)/383(3.24)	None

[a] Calculated at DFT B3LYP/6-311++G(3d,f,2p) level in vacuum; [b] HOMO–LUMO/HOMO–1–LUMO gaps; [c] TD-DFT calculated (nstates = 8) using B3LYP/6-311++G(3d,f,2p) or CAM-B3LYP/6-311++G(2d,p) in vacuum; [d] Group of Symmetry.

10.1002/chem.202004328

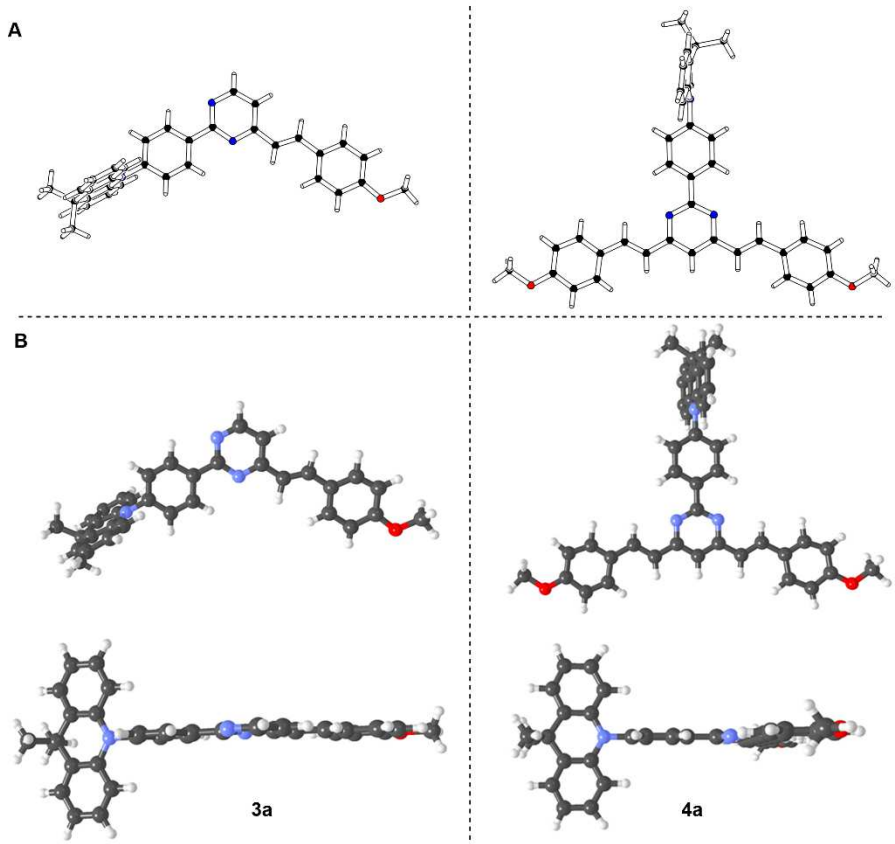

Figure 3: X-ray (A) and DFT-optimized (B) geometries of chromophores **3a** and **4a**.

The DFT-optimized geometry of representative chromophores **3a** and **4a** is shown in Figure 3. Both structures are almost identical to the aforementioned X-ray analyses and show perpendicular arrangement of the acridan moiety towards the residual π-system. The calculated torsion angles between the acridan and pyrimidine rings are 86 and 90°, respectively. The optimized structures also revealed significant differences between the methoxy and *N*,*N*-diphenylamino substituted derivatives **a/b** and **c**, the latter possesses no symmetry. Compared to mono-substituted styryl pyrimidines **3**, the ground state dipole moments of distyryl derivatives **4** are diminished. However, *N*,*N*-diphenylamino substituents in **4c** impart unsymmetry and enlarge the dipole moment up to 5.3 D. The calculated energies of the HOMO and the LUMO are listed in Table 2. There are no significant differences between the particular values, and, therefore, the HOMO–LUMO gaps ΔE fall within a short range of 2.61-2.80 eV. The gap is almost independent on the appended peripheral methoxy

10.1002/chem.202004328

and *N*,*N*-diphenylamino donors (**a**–**c**), which would imply that these are not engaged in the ICT transition that is responsible for the longest wavelength absorption band as will be discussed below.

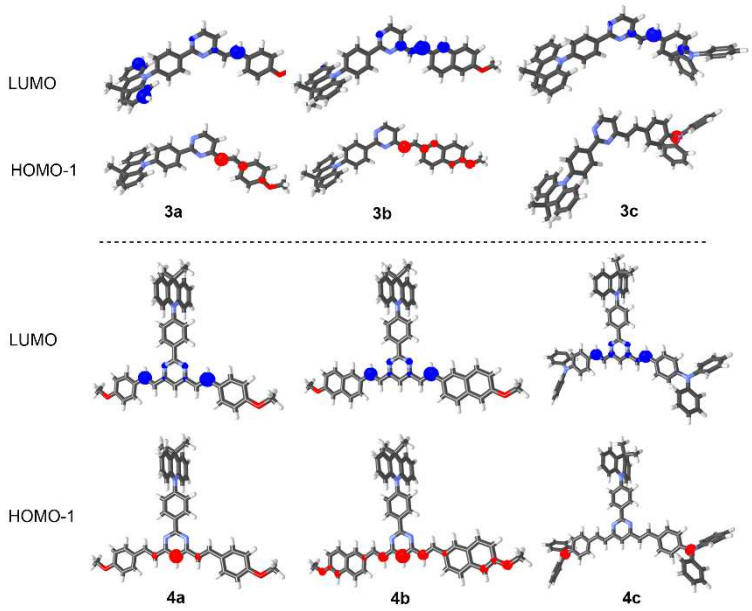

Figure 4: HOMO–1 (red) and LUMO (blue) localizations in chromophores **3** and **4**.

The relevant HOMO–1/LUMO localizations in chromophores **3** and **4** are shown in Figure 4, for complete visualization of the frontier molecular orbitals see Figures S9-10. As a dominant feature, the HOMO always occupies the acridan nitrogen atom, whereas the LUMO is spread over the pyrimidine central ring and the appended olefinic linker(s). On the contrary, the HOMO–1 is localized over the methoxy- or *N*,*N*-diphenylamino-terminated styryl branch(es). In **3a**–**c**, the HOMO–2 occupies again the phenylacridan branch, whereas in **4a**–**c** it remains localized similarly to HOMO–1. The higher unoccupied molecular orbitals LUMO+1 and LUMO+2 are generally localized over the central pyrimidine ring and the adjacent π-system or may be shifted towards acridan moiety.

The electronic absorption spectra were calculated at TD-DFT level employing two functionals: convenient CAM-B3LYP/6-311++G(2d,p) as well as B3LYP/6-311++G(3d,f,2p). The spectra are shown in Figures S11 and S12; the calculated

positions of the longest-wavelength absorption maxima are listed in Table 2. Compared to the experimental values, the B3LYP slightly overestimates λ_{max} values ($\Delta\lambda_{max}$ = 10-42 nm), while the CAM-B3LYP behaves conversely ($\Delta\lambda_{max}$ = 12-49 nm). A dependency of both calculated values revealed tighter correlation of the B3LYP values (Figure S13) and, therefore, we consider the B3LYP more appropriate for describing electronic properties of **3** and **4**. This is in agreement with the recent observation on heterocyclic push-pull molecules made by Tang et al.[30] Compared to the experimental spectra measured in CH_2Cl_2, the calculated spectra possess the same features and bands (Figure S11). An inspection of the particular transitions and oscillator strengths (Table S4) revealed that the longest-wavelength absorption band is exclusively generated by the HOMO–1→LUMO transition. Pure HOMO→LUMO transition, a typical feature of push-pull molecules,[31] has been found within a range of 495–529 nm but possess zero oscillator strength. Considering the HOMO–1 localization over the methoxy and *N*,*N*-diphenylamino peripheral donors, their D-A interaction with the central pyrimidine acceptor (LUMO) accounts for the intramolecular charge transfer (ICT) and also explains the observed bathochromic shift of the longest-wavelength absorption maxima when going from **3a** to **3c** or **4a** to **4c**. It is also indicative that, compared to methoxy group, the *N*,*N*-diphenylamino donor is strongly engaged in the ICT. Correlation of the λ_{max}^{DFT} values (Table 2) against the experimental λ_{max} (Table 3) clearly demonstrate very tight dependence of these two quantities. On the contrary, there is no correlation between the HOMO–LUMO gap and the experimentally obtained optical gap (see Figure S14). Apart from the longest wavelength HOMO–1→LUMO transition, the remaining minor transitions in the DFT calculated absorption spectra (Figure S11) mostly involve HOMO–1→LUMO+1 (**3a**–**c**) and also HOMO–2→LUMO (**4a**–**c**) contributions (Table S4).

An inspection of geometries of the calculated singlet and triplet states of model **3a** revealed very small spatial differences of both states. Whereas the acridan moiety remained

perpendicularly arranged in both excited states, a slight enlargement of the C=C bond of the styryl moiety occupied by the LUMO was observed (1.328 and 1.388 A for the ground and triplet states). The remaining frontier molecular orbitals are positioned analogously to the ground state. This imply a relatively small barrier between both singlet and triplet states.

Overall, chromophores **3** and **4** possess the HOMO isolated on the out-of-plane acridan and the initial absorption properties are rather controlled by peripheral methoxy and *N*,*N*-diphenylamino donors bearing the HOMO–1. Whereas the *N*,*N*-diphenylamino group in chromophores **c** brings molecular unsymmetry and strong D-A interaction, the methoxy group is weaker donor and chromophores **a** and **b** possess C_s and C_{2v} group of symmetry, respectively.

Photophysical properties

Photophysical properties in solutions. The UV/Vis and photoluminescence (PL) properties of compounds **3** and **4** were initially measured in CH_2Cl_2 and the results are presented in the SI (Table S5). These compounds show absorption properties similar to other pyrimidines without C2-substituents,[21a-b] but surprisingly almost no emission was detected for the methoxy derivatives **3a**–**b** and **4a**–**b**. On the other hand, the *N*,*N*-diphenylamino derivatives **3c** (PL λ_{max} = 531 nm, Φ_F = 0.75) and **4c** (PL λ_{max} = 552 nm, Φ_F = 0.94) are highly luminescent in CH_2Cl_2. Measurements have been performed also in the nonpolar *n*-heptane, the results are presented in Table 3. As an example, the normalized spectra of the compounds **3** are shown in Figure 5 (the corresponding spectra of chromophores **4** are shown in Figure S15). Compared to methoxy derivatives **3a** and **4a**, the *N*,*N*-diphenylamino derivatives **3c** and **4c** exhibited significantly red-shifted absorption and emission. The replacement of the phenyl linker by naphthyl one (**3b** vs. **3a** or **4b** vs. **4a**) caused a red shift of the absorption maxima ($\Delta\lambda_{max}$ = 30/12 nm), whereas the emission spectra are almost identical. In *n*-heptane, a dramatic increase of the emission intensity was observed for methoxy derivatives suggesting AIE

10.1002/chem.202004328

phenomena, aggregation of such choromophores being plausible in this solvent even at low concentration. In contrast, the quantum yields of chromophores **3c** and **4c** in *n*-heptane are significantly reduced compared to the values in CH_2Cl_2 solution. Deoxygenating the solutions slightly increases the emission quantum yields.

Table 3: UV/Vis and PL data in *n*-heptane.

Compd[a]	UV/vis λ_{max}, nm (ε, $mM^{-1}\cdot cm^{-1}$)	PL λ_{max}, nm	Solidst. λ_{max}, nm	Φ_F[b]	Φ_F (deox.)[c]	Stokes shift cm^{-1}
3a	337 (29.4)	432	471	0.11	0.15	6525
3b	368 (24.5)	429	471	0.09	0.13	3864
3c	396 (30.7)	444	521	0.37	0.40	2730
4a	383 (24.3)	426	474	0.06	0.08	2635
4b	395 (48.8)	435	508	0.22	0.29	2328
4c	432 (53.6)	460	535	0.63	0.74	1409

[a] All spectra were recorded at room temperature at $c = 0.9 \times 10^{-5}$ M to 1.02×10^{-5}. [b] Fluorescence quantum yield (±10%) determined relative to 9,10-bisphenylethynylanthracene in cyclohexane (Φ_F = 1.00).[32] [c] Deoxygenated solutions were prepared by bubbling N_2 through the solutions.

10.1002/chem.202004328

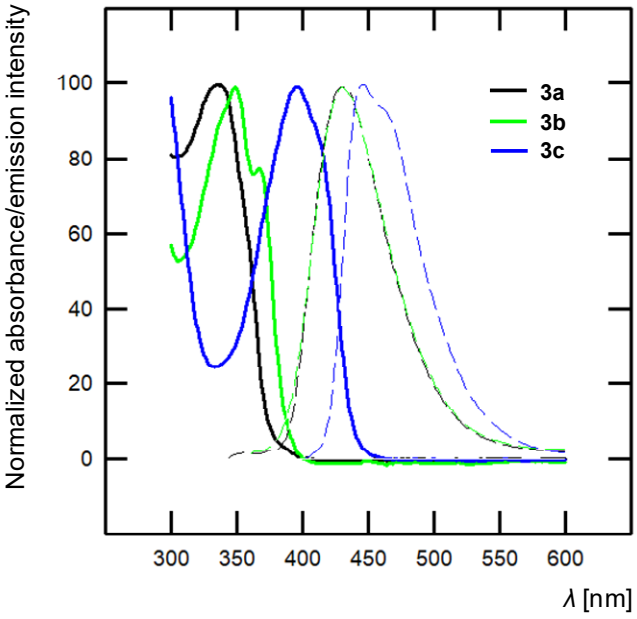

Figure 5: Normalized absorption (solid lines) and emission spectra (dashed lines) of compounds **3a** (black), **3b** (green) and **3c** (blue) in *n*-heptane solution.

As well documented for other donor-substituted styrylpyrimidine derivatives,[21] *N*,*N*-diphenylamino derivatives **3c** and **4c** exhibit large positive emission solvatochromism (Figures 6 and S16–S17). This phenomenon, characteristic of push-pull derivatives is explained by the stabilization of the highly polar emitting excited state by polar solvents.[33]

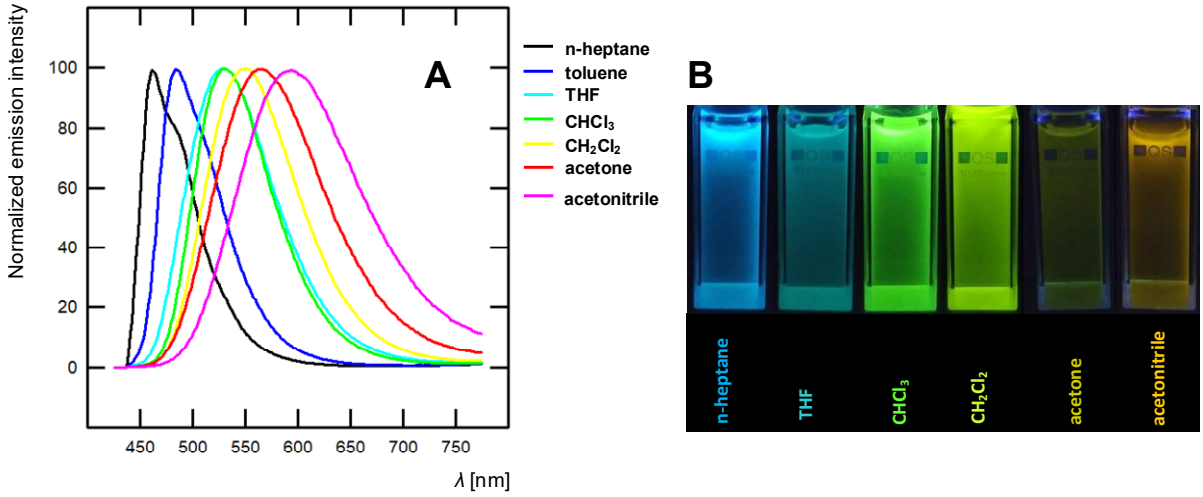

10.1002/chem.202004328

Figure 6: A) Normalized emission spectra of **4c** in different aprotic solvents, B) Fluorescence color changes experienced by **4c** in various solvents. Picture was taken in the dark upon irradiation with a handheld UV lamp (λ_{em} = 254 nm).

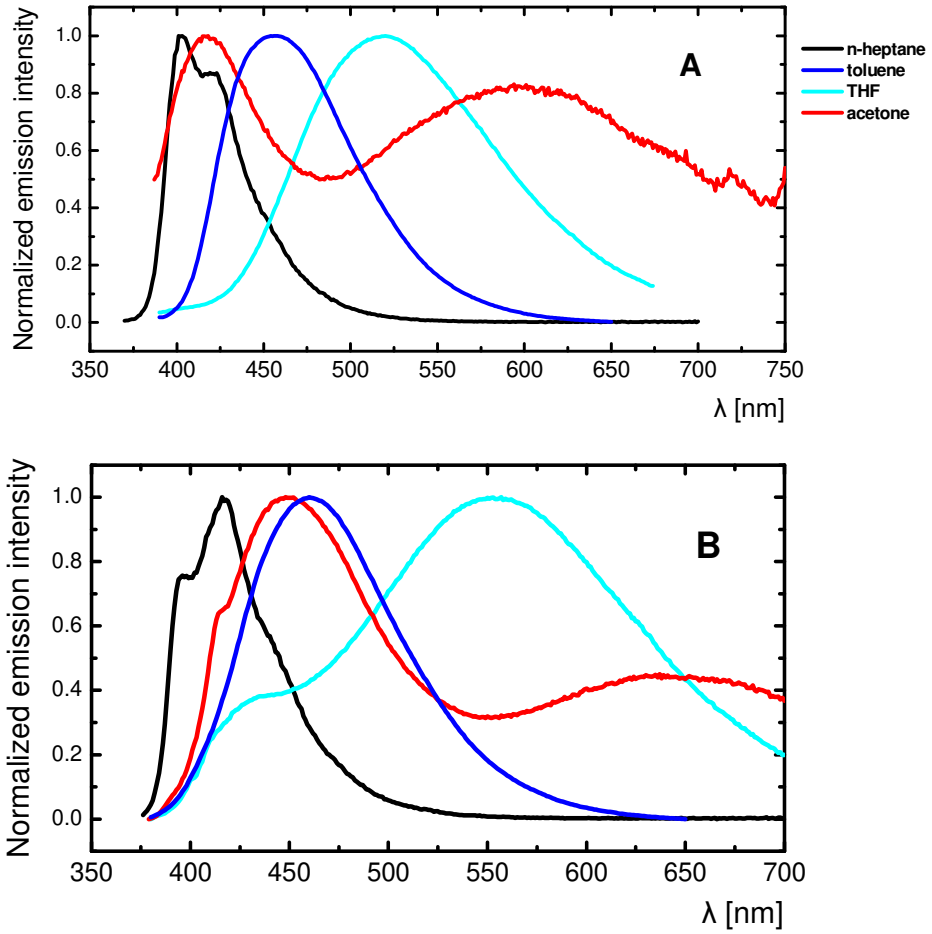

Figure 7: Normalized emission spectra of **3a** (A) and **4a** (B) in different aprotic solvents.

However, the methoxy derivatives **3a**, **3b** and **4a**, **4b** do not exhibit typical solvatochromic behavior as observed for **3c** and **4c**. The fluorescence spectra of **3a** become red-shifted and broader upon increasing the solvent polarity from *n*-heptane to toluene and to THF, which is indicative of emission originating from an excited state with ICT characteristics. However, when increasing further the polarity to acetone, a dual emission is observed (Figure 7A). It consists of a broad red-shifted band, emitted from a state with ICT or Twisted-ICT (TICT) nature, that exhibits expected solvatochromic behavior and a blue-shifted band caused by

10.1002/chem.202004328

fluorescence of the locally excited (LE) state, which became significant due to a very low intensity of the ICT/TICT emission. For **4a**, the dual emission is observable even in THF with the LE state exhibiting a high-energy fluorescence shoulder (Figure 7B). The LE emission is dominant in acetone. Chromophores **3b** and **4b** exhibit a simultaneous dual emission from the LE and ICT/TICT states in THF, while in acetone, the emission from the solvated LE band prevails (Figure S18). The above mentioned solvatochromic behavior of chromophores **3** and **4** is indicative of significant differences in the fundamental photophysics of *N*,*N*-diphenylamino and methoxy derivatives which is based on the fact that these electron donating groups participate in ICT (and not the acridine) as revealed by the DFT calculations. The differences in photophysics will be further analyzed by investigating the excited state dynamics.

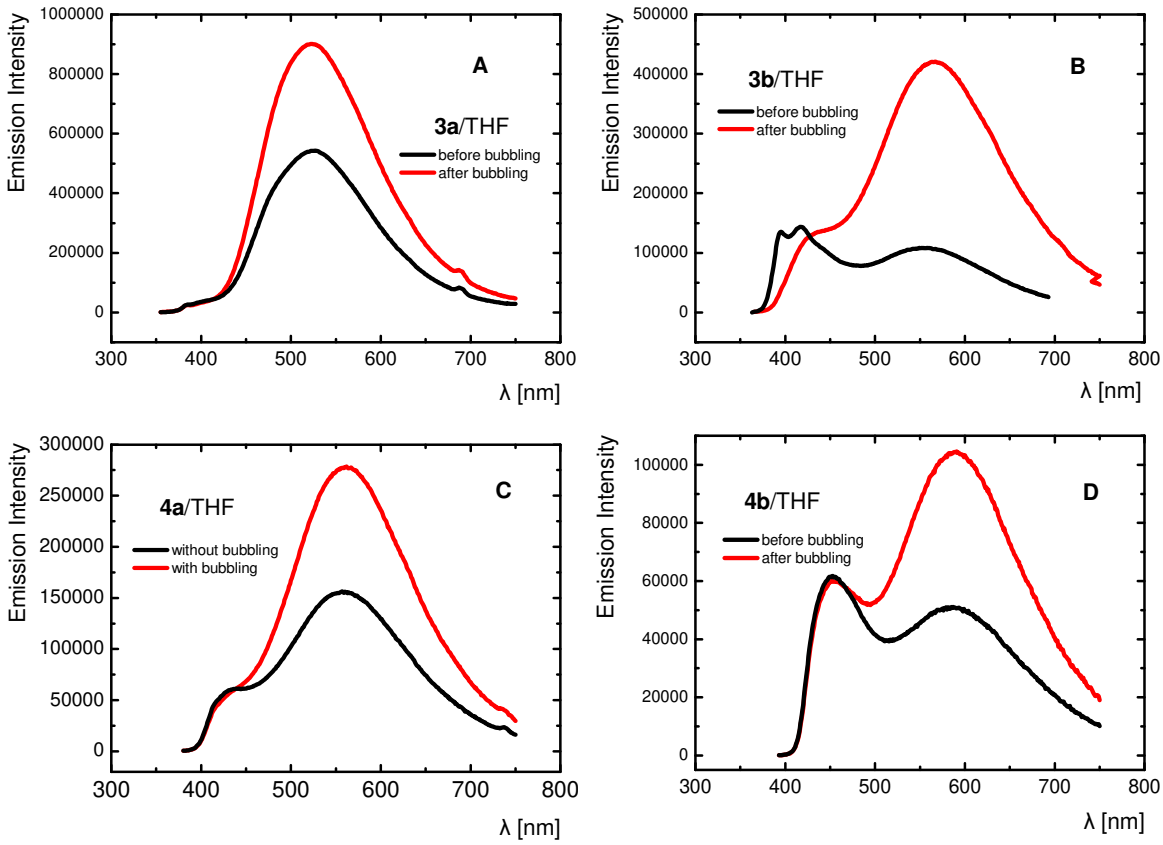

Figure 8: Emission spectra of **3a**, **3b** and **4a**, **4b** in THF before and after bubbling with N_2.

The effect of bubbling with N_2 on the fluorescence spectra was investigated in THF as shown in Figures 8 and S19. For **3a**–**b** and **4a**–**b** it is obvious that the intensity of the low energy broad emission peak increases almost twice upon bubbling, which suggests that this emission band is quenched by oxygen (Figure 8).[34] On the other hand, the high energy peak experiences almost negligible changes upon bubbling. In general, oxygen acts as a fluorescence quencher for both LE and ICT states but affects more dramatically the longer-lived states, this being a first evidence that in the methoxy derivatives, the ICT state is highly stabilized with long lifetime. The fluorescence spectra of *N*,*N*-diphenylamino derivatives, which as mentioned before showed single peak independently on the solvent polarity (Figures 6 and S16), exhibited negligible changes upon bubbling (Figure S19) which is again indication for the differences in the nature of the emitting ICT states between the methoxy and *N*,*N*-diphenylamino derivatives.

Excited state dynamics were investigated at both emission bands of **3** and **4** in THF; the results before and after bubbling with N_2 are shown in Figures 9 and S20. Compared to methoxy derivatives, the decays of the *N*,*N*-diphenylamino compounds **3c** and **4c** (Figure S20 B and D) exhibited again a different behavior. Both **3c** and **4c** possess 2.45 ns average decay lifetimes, which is typical for compounds emitting from an ICT state. Furthermore, the lifetimes barely depend on bubbling with N_2 (the lifetimes of both **3c** and **4c** increased to 2.75 ns after bubbling). The decays of the methoxy compounds are complex and cannot be explained by a typical ICT emitting state. The decays also differ for the high- and low-energy bands. For example, for **4b**, at the high-energy band, the dynamics are very fast (Figure 9) with lifetimes within the IRF of our system (< 80 ps). Such decay dynamics is expected from a molecule having very small quantum yield in solvents of medium polarity. However, the decays at the low-energy band exhibit a very fast component (which is again < 80 ps, ~ 90% amplitude), followed by a longer one (within the order of 10 ns, ~ 10% amplitude). The long

10.1002/chem.202004328

component becomes even more retarded after bubbling with N_2 (within the order of 30 ns, ~10% amplitude). After exposure to air, the lifetime of the long component again decreases. These observations imply that methoxy chromophores have two contributions in emission with different origin. The high-energy emission band originates from fluorescence of the LE state, has very small quantum yield and is not affected by bubbling. The low-energy emission band contains LE fluorescence as well as long-lived fluorescence from a highly stabilized ICT state , which is strongly dependent on bubbling due to its long lifetime.[35]

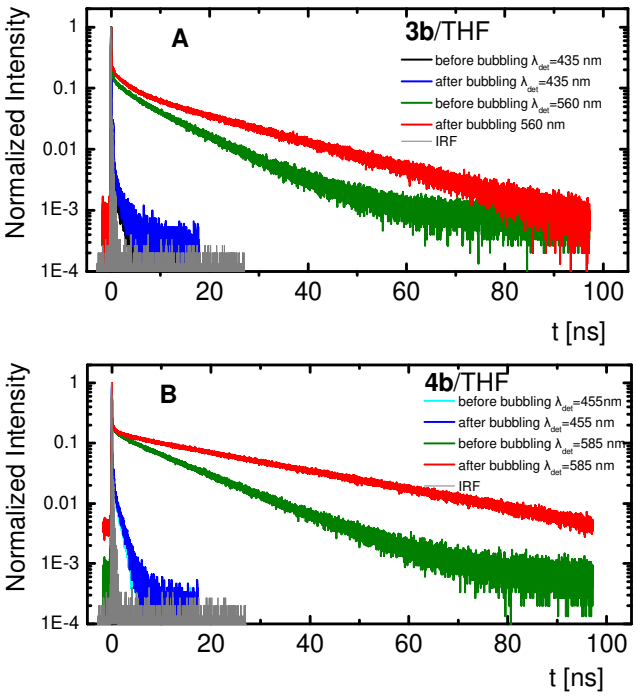

Figure 9: Emission dynamics of **3b** and **4b** in THF before and after bubbling with N_2 detected at both the high- and low-energy emission bands. The instrument's response function is also shown.

The contribution of the long-lived part of the fluorescence depends on the solvent used. In *n*-heptane solutions, where a single emission band is observed, the dynamics is only very weakly dependent on bubbling (Figure S21). This means that in this low polarity solvent, the emission is mainly due to a singlet LE fluorescence without contribution from ICT states. In *n*-heptane, in which the excited state faces a very weak solvation reaction field, the ICT/TICT

10.1002/chem.202004328

formation is endergonic , while in THF which is a solvent of medium polarity the energy of the ICT state is reduced, aided by means of solvation, thus ICT population is energy efficient.

As written before, AIE is an important characteristic for chromophores with potential applications in lighting devices. In order to study potential AIE properties of compounds **3** and **4**, their emission spectra were recorded in THF-water mixtures of different ratio. Figure 10 shows representative examples for **3b** and **3c**, the remaining spectra are provided in the SI (Figures S22–S25). In the case of the methoxy derivative **3b**, the dual emission behavior observed in THF disappears upon adding 10% of water and only the emission of the LE state remains, which slightly shifts to the red for larger amounts of water due to the increase of solvent polarity. No significant increase of the emission intensity is observed with water fraction below 80%. A progressive increase of the emission intensity accompanied by a significant red-shift of the emission band is observed for higher portion of water. However, further increasing the water content from 80% to 97% caused a blue shift. For **3c**, increasing the water fraction up to 60%, induces a progressive decrease of the emission intensity with a slight red shift of the emission maxima. This phenomenon is attributed to the increased polarity of the media. A slight rebound of the emission accompanied by a blue-shift of the maxima was detected when increasing the water content to 80%. In the solutions with more than 80% of water, the emission intensity decreases again.

10.1002/chem.202004328

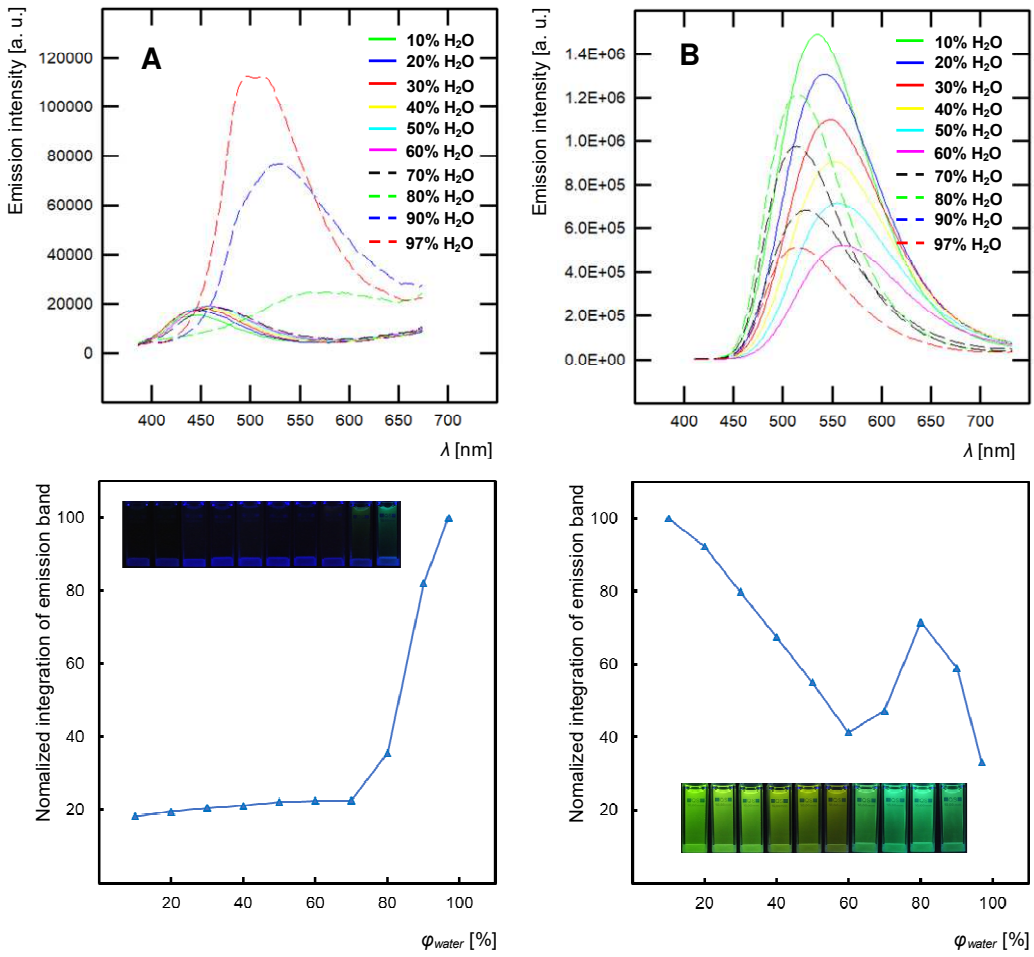

Figure 10: Fluorescence emission spectra of **3b** (A) and **3c** (B) ($c = 1 \times 10^{-5}$ M) in THF/water mixture. Integration of emission band versus volume percent of water in mixtures of THF/water of **3a** and **3c**. Insert pictures were taken in the dark upon irradiation with a hand-held UV lamp ($\lambda_{em} = 254$ nm).

As a further investigation on the AIE properties the excited state dynamics were examined upon increasing the amount of the poor solvent. Since in AIE chromophores, aggregation is expected to suppress non-radiative processes, the lifetime in such systems is expected to increase and this will be a valuable tool in order to assess the potential of these molecules for solid state lighting applications. In the herein studied acridan molecules, the out-of-plane rotation of the acridan moiety is expected to play the role of an energy consuming process reducing the luminescence intensity. Aggregation is considered to hinder this process and this motion. This hypothesis is confirmed by the intense emission band observed for **3a** at 402 nm

10.1002/chem.202004328

in glycerol, a viscous solvent hindering molecular motion (Figure S26). Corresponding results for the dynamics of compounds **3b** and **4b** in THF-water mixtures, are shown in Figures 11 and S27 respectively. Indeed, the time resolved emission results depict an increase of the average lifetime for **3b** and **4b** that takes place upon increasing the amount of water. Specifically, for **3b**, the amplitude average lifetime increases from < 0.050 ns for 20% water to 2.7 ns for 95% water while for **4b**, the lifetime increases from < 0.050 ns to 3.6 ns (Tables S6 and S7).

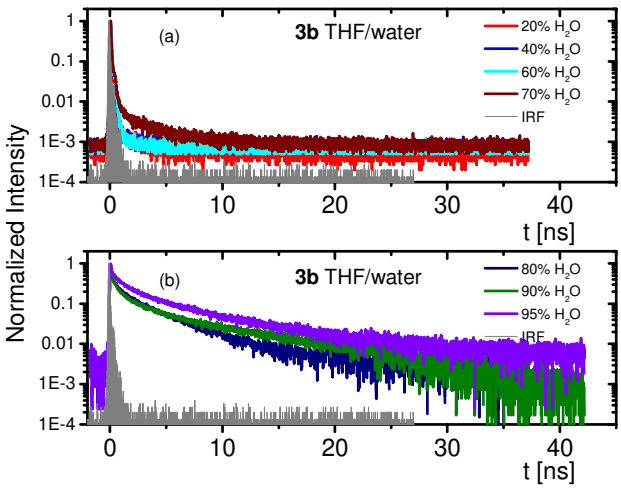

Figure 11. Emission dynamics of **3b** ($c = 1 \times 10^{-5}$ M) in THF/water mixtures (a) 20-70 % and (b) 80-95 %.

Photophysical properties in solid state. The solid state (powder) emission spectra of compounds in series **3** and **4** were also measured. The emission maxima are summarized in Table 3 while Figure 12 shows their normalized spectra and emission color. The methoxy derivatives **3a–b** and **4a–b** exhibited blue emission whereas the *N*,*N*-diphenylamino coumpounds **3c** and **4c** showed green emission.

10.1002/chem.202004328

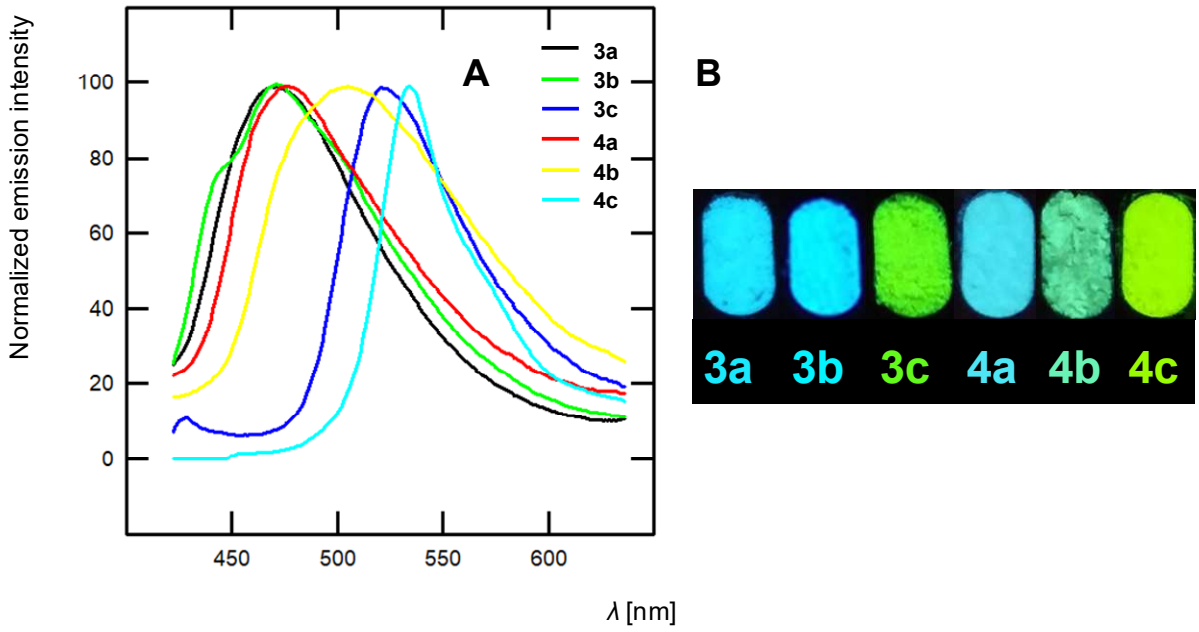

Figure 12: A) Normalized emission spectra of solid state compounds **3a–c** and **4a–c**. B) Fluorescence color of compounds **3** and **4** (powder). Picture was taken in the dark upon irradiation with a handheld UV lamp (λ_{em} = 254 nm).

The emission spectra of thin films, prepared by spin-coating, provided further important results on the differences between the methoxy and diphenylamino chromophores (Figure 13). The methoxy compounds **a** and **b** clearly exhibited dual emission behavior with the emission spectra covering almost the whole visible region. The dual emission is more pronounced for **3a** and **3b** where two peaks are clearly identified. The emission spectra of **4a** and **4b** feature a high-energy shoulder instead of two separate peaks. The corresponding chromaticity coordinates, that are not far from pure white light, are provided in Table 4. On the contrary, the *N*,*N*-diphenylamino compounds **c** showed a single emission peak attributed to the emission from their S_1 state. The two emission bands of the methoxy compounds in neat film clearly have different origin, similarly to their THF solutions. The low-energy fluorescence band involves long-lived ICT state as revealed by the emission decays with long dynamics (for **3a** and **3b** see Figure S28). The broad white light spectrum of their neat films render

10.1002/chem.202004328

these materials potential candidates for use as single emissive layer in white organic light emitting diodes (WOLED).

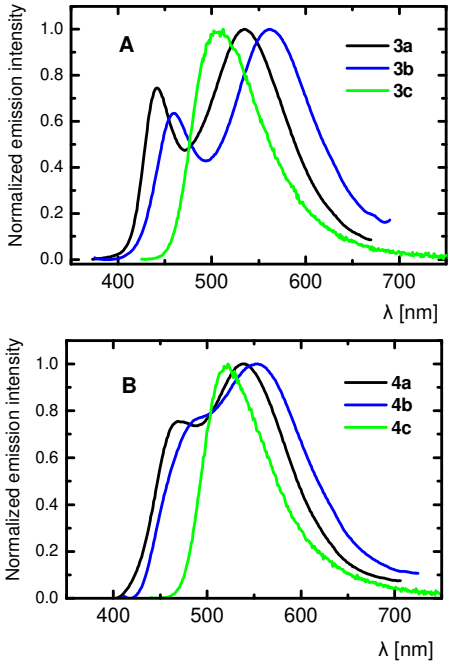

Figure 13: Emission spectra of neat thin films of flurophores **3** and **4**.

Table 4: CIE chromaticity coordinates (x, y) for compounds **3** and **4.**

3a	**3b**	**3c**	**4a**	**4b**	**4c**
(0.28, 0.40)	(0.35, 0.41)	(0.27, 0.54)	(0.29, 0.42)	(0.35, 0.45)	(0.32, 0.60)

Conclusions

We have designed multipodal D-π-A(-π-D)$_n$ (n = 1-2) molecules based on pyrimidine central acceptor and two/three peripheral donors of different electronic and spatial nature. Whereas the acridan moiety linked *via* 1,4-phenylene linker at C2 of the pyrimidine ring possesses out-of-plain arrangement, the peripheral methoxy or *N*,*N*-diphenylamino groups interacts directly with the pyrimidine acceptor. The quantum-chemical calculations revealed that despite the HOMO is localized on the acridan moiety, it is completely isolated and does not affect the fundamental absorption properties. These are fully affected by the peripheral methoxy and *N*,*N*-diphenylamino groups bearing HOMO–1. The *N*,*N*-diphenylamino strong donor in

compounds **3c** and **4c** caused formation of an intense single band emission in both solution and solid state. It showed positive solvatochromism attributed to the ICT from the NPh_2 group to the pyrimidine core (HOMO–1→LUMO transition). On the other hand, the methoxy derivatives are poorly emissive in moderately polar solvents such as CH_2Cl_2 but exhibit intense AIE. Dual emission has been observed in THF as well as in neat thin film and is attributed to the LE and ICT/TICT excited states with the lowest energy emission band having long lifetime. The dual fluorescence observed for **3a**–**b** and **4a**–**b** thin films makes these materials highly promising for the development of WOLEDs.

Experimental section

General Conditions. Reagents and solvents were reagent-grade and were purchased from Sigma Aldrich or TCI Europe and used as received. 4-(9,9-Dimethyl-9,10-dihydroacridine)phenylboronic acid pinacol ester was prepared according to literature procedure.[36] NMR spectra were acquired at room temperature at 400/100 MHz with a Bruker AVANCE III or 500/125 MHz with Bruker Ascend^{TM}. Chemical shifts are given in parts per million relative to TMS (^{1}H, 0.0 ppm) and $CDCl_3$ (^{13}C, 77.0 ppm). Acidic impurities in $CDCl_3$ were removed by treatment with anhydrous K_2CO_3. High resolution MALDI MS spectra were measured on a MALDI mass spectrometer equipped with nitrogen UV laser (337 nm, 60 Hz) and quadrupole analyser (positive-ion mode over a normal mass range (*m/z* 50-2000) with resolution 100 000 at *m/z* = 400). *Trans*-2-[3-(4-*tert*-butylphenyl)-2-methyl-2-propenylidene]malononitrile (DCTB) was used as a matrix. Mass spectra were averaged over the whole MS record for all measured samples.

Photophysical characterization: The absorption spectra of the samples in solutions and films were detected with a Jasco V-650 while the emission spectra were detected by a Horiba Fluoromax spectrophotometer respectively. UV-vis and fluorescence spectra were recorded

using standard 1 cm quartz cells. Compounds were excited at their absorption maxima (band of lowest energy) to record the emission spectra. The Φ_F values were calculated using a well-known procedure with 9,10-diphenylethynylanthracene in cyclohexane as standard (Φ_F = 1). Stokes shifts were calculated by considering the lowest energetic absorption band. The detection of the dynamics has been carried out via a Time Correlated Single Photon Counting (TCSPC) technique (Fluotime 200 spectrometer Picoquant). The excitation source was a diode laser at 400 nm emitting 60 ps pulses. The resolution was ~80 ps however shorter lifetimes can be calculated by fitting the experimental results with multi-exponential functions convoluted with the instrument's response function.

DSC: Thermal properties of molecules **3** and **4** were investigated by DSC measurements with a Mettler-Toledo STARe System DSC 2/700 equipped with FRS 6 ceramic sensor and cooling system HUBER TC100-MT RC 23. Thermal behavior of the target chromophores were measured in open aluminous crucibles under N_2 inert atmosphere. DSC curves were determined with a scanning rate of 3 °C/min within the range 25-500 °C.

X-Ray Structural Analysis: Single-crystal X-ray-diffraction data were obtained from a D8 VENTURE Bruker AXS difractometer equipped with a (CMOS) PHOTON 100 detector, using Mo-Kα radiation (λ = 0.71073 Å, multilayer monochromator) at T = 150 K. Structures of the crystals were solved by dual-space algorithm using the SHELXT program,[37] and then refined with full-matrix least-squares methods based on F^2 (SHELXL program).[38] All non-hydrogen atoms were refined with anisotropic atomic displacement parameters. H atoms were finally included in their calculated positions and treated as riding on their parent atom with constrained thermal parameters. Drawings were produced using ORTEP-3. CCDC-200148 (**3a**), CCDC-200147 (**4a**) and CCDC-200149 (**4c**) contain supplementary crystallographic data. These data can be obtained free of charge from the Cambridge Crystallographic Data Centre via www.ccdc.cam.ac.uk/data_request/cif.

General procedure for Suzuki-Miyaura cross-coupling reaction: 4-(9,9-Dimethyl-9,10-dihydroacridine)phenylboronic acid pinacol ester (1 equiv) and 2-chloro-4-methylpyrimidine or 2-chloro-4,6-dimethylpyrimidine (1 equiv) were dissolved in THF (20 mL), and nitrogen was bubbled trough the solution for 10 min. $Pd(PPh_3)_4$ (0.05 equiv) and 20% aqueous Na_2CO_3 (5 mL) were added, and then the reaction was stirred under nitrogen atmosphere at 65 °C for 15h. The reaction mixture was cooled to room temperature and CH_2Cl_2/aqueous NH_4Cl (1:1, 50 mL) was added. The organic layer was separated, and the aqueous layer was extracted with additional CH_2Cl_2 (2 × 25 mL). The combined organic extracts were dried over anhydrous Na_2SO_4 and solvent was evaporated under reduced pressure. The residue was purified by column chromatography (SiO_2; EtOAc/hexane 9:1).

General procedure for Knoevenagel condensation: Aldehyde (1 equiv) and **1** (1 equiv) or **2** (0.5 equiv) were added in 5 M aqueous NaOH (20 mL) containing aliquat 336 (0.1 equiv). The suspension was stirred at 110 °C for 3h and then cooled to room temperature. The precipitate was filtered off, washed with water, dried under reduced pressure, and purified by column chromatography (SiO_2; indicated solvents) and/or by recrystallization from CH_2Cl_2/hexane.

2-[4-(9,9-Dimethyl-9,10-dihydroacridine)phenyl]-4-methylpyrimidine (**1**): Synthesized from 2-chloro-4-methylpyrimidine (83 mg, 0.64 mmol) and boronic acid pinacol ester (265 mg, 0.64 mmol) following the general procedure for Suzuki-Miyaura cross-coupling reaction. Yield 138 mg (57 %); pale yellow solid; R_f = 0.2 (SiO_2; hexane/EtOAc 9:1); ^{1}H NMR (400 MHz, $CDCl_3$) δ = 8.71 (d, ^3J = 5 Hz, 1H), 8.69–8.67 (m, 2H), 7.48–7.46 (m, 4H), 7.13 (d, ^3J = 5 Hz, 1H), 6.99–6.91 (m, 4H), 6.36–6.34 (m, 2H), 2.64 (s, 3H), 1.71 (s, 6H) ppm. ^{13}C NMR (125 MHz, $CDCl_3$) δ = 167.69, 164.00, 157.13, 143.48, 140.82, 137.95, 131.63, 130.92, 130.11, 126.50, 125.40, 120.74, 119.04, 114.24, 36.11, 31.46, 24.62 ppm. HR-MALDI-MS (DCTB) m/z calcd for $C_{25}H_{20}N_3$ [M-CH_3^+] 362.1652, found 362.1640.

2-[4-(9,9-Dimethyl-9,10-dihydroacridine)phenyl]-4,6-methylpyrimidine (**2**): Synthesized from 2-chloro-4,6-dimethylpyrimidine (111 mg, 0.78 mmol) and boronic acid pinacol ester (321 mg, 0.78 mmol) following the general procedure for Suzuki-Miyaura cross-coupling reaction. Yield 166 mg (54 %); pale yellow solid; R_f = 0.3 (SiO_2; hexane/EtOAc 9:1); ^{1}H NMR (400 MHz, $CDCl_3$) δ = 8.73–8.71 (m, 2H), 7.54–7.51 (m, 4H), 7.07 (s, 1H), 7.04–6.97 (m, 4H), 6.42–6.40 (m, 2H), 2.66 (s, 6H), 1.78 (s, 6H) ppm. ^{13}C NMR (125 MHz, $CDCl_3$) δ = 167.21, 163.87, 143.22, 131.58, 130.99, 130.04, 126.49, 125.40, 120.69, 118.42, 114.26, 36.11, 31.52, 24.36 ppm. HR-MALDI-MS (DCTB) m/z calcd for $C_{26}H_{22}N_3$ [M-CH_3^+] 376.1808, found 376.1796.

(E)-2-[4-(9,9-Dimethyl-9,10-dihydroacridine)phenyl]-4-[(4-methoxyphenyl)ethenyl]pyrimidine (**3a**): Synthesized from compound **1** (138 mg, 0.36 mmol) and 4-methoxybenzaldehyde (50 mg, 0.36 mmol) following the general procedure for Knoevenagel condensation. The crude product was purified by recrystallization. Yield 126 mg (70 %); yellowish solid; R_f = 0.5 (SiO_2; CH_2Cl_2); mp: 204°C. ^{1}H NMR (500 MHz, $CDCl_3$) δ = 8.78–8.75 (m, 3H), 8.02 (d, ^3J = 16 Hz, 1H), 7.63–7.61 (m, 2H), 7.50–7.47 (m, 4H), 7.23–7.22 (m, 1H), 7.04 (d, ^3J = 16 Hz, 1H), 6.99–6.93 (m, 6H), 6.38–6.37 (m, 2H), 3.87 (s, 3H), 1.72 (s, 6H) ppm. ^{13}C NMR (125 MHz, $CDCl_3$) δ = 163.95, 163.09, 160.89, 157.81, 143.49, 140.85, 138.12, 137.14, 131.60, 130.99, 130.12, 129.41, 128.57, 126.53, 125.40, 123.79, 120.74, 116.53, 114.49, 114.27, 55.54, 36.13, 31.46 ppm. HR-MALDI-MS (DCTB) m/z calcd for $C_{33}H_{26}N_3O$ [M-CH_3^+] 480.2070, found 480.2058.

(E)-2-[4-(9,9-Dimethyl-9,10-dihydroacridine)phenyl]-4-[(6-methoxynaphtalen-2-yl)ethenyl]pyrimidine (**3b**): Synthesized from compound **1** (102 mg, 0.27 mmol) and 6-methoxy-2-naphtalenaldehyde (51 mg, 0.27 mmol) following the general procedure for Knoevenagel condensation. The crude product was purified by column chromatography (hexane/EtOAc 7:3). Yield 109 mg (74 %); yellowish solid; R_f = 0.5 (SiO_2; hexane/EtOAc

7:3); mp: 199 °C. ^{1}H NMR (400 MHz, $CDCl_3$) δ = 8.81–8.78 (m, 3H), 8.20 (d, ^{3}J = 16 Hz, 1H), 7.99 (br s, 1H), 7.83–7.77 (m, 3H), 7.52–7.47 (m, 4H), 7.28–7.16 (m, 4H), 7.01–6.93 (m, 4H), 6.41–6.38 (m, 2H), 3.95 (s, 3H), 1.73 (s, 6H) ppm. ^{13}C NMR (100 MHz, $CDCl_3$) δ = 164.02, 162.96, 158.72, 157.92, 143.60, 140.89, 138.11, 137.76, 135.40, 131.61, 131.25, 131.03, 130.18, 130.13, 129.13, 129.05, 127.62, 126.54, 125.40, 125.26, 124.42, 120.77, 119.53, 116.69, 114.31, 106.16, 55.53, 36.15, 31.47 ppm. HR-MALDI-MS (DCTB) m/z calcd for $C_{37}H_{28}N_3O$ [M-CH_3^+] 530.2227, found 530.2221.

(E)-2-[4-(9,9-Dimethyl-9,10-dihydroacridine)phenyl]-4-[(4-diphenylaminophenyl)ethenyl]pyrimidine (**3c**): Synthesized from compound **1** (228 mg, 0.60 mmol) and 4-diphenylaminobenzaldehyde (164 mg, 0.60 mmol) following the general procedure for Knoevenagel condensation. The crude product was purified by column chromatography (CH_2Cl_2). Yield 182 mg (48 %); yellow solid; R_f = 0.8 (SiO_2; CH_2Cl_2); mp: 375 °C (dec.). ^{1}H NMR (400 MHz, $CDCl_3$) δ = 8.87–8.84 (m, 3H), 8.09 (d, ^{3}J = 16 Hz, 1H), 7.61–7.56 (m, 6H), 7.41–7.01 (m, 18H), 6.49–6.47 (m, 2H), 1.81 (s, 6H) ppm. ^{13}C NMR (100 MHz, $CDCl_3$) δ = 163.92, 163.08, 157.70, 149.22, 147.21, 143.50, 140.85, 138.13, 137.04, 131.53, 130.97, 130.13, 129.56, 129.16, 128.90, 126.51, 125.35, 123.86, 123.76, 122.38, 120.74, 116.43, 114.28, 36.10, 31.44 ppm. HR-MALDI-MS (DCTB) m/z calcd for $C_{44}H_{33}N_4$ [M-CH_3^+] 617.2700, found 617.2689.

(E,E)-2-[4-(9,9-Dimethyl-9,10-dihydroacridine)phenyl]-4,6-bis[(4-methoxyphenyl)ethenyl]pyrimidine (**4a**): Synthesized from compound **2** (158 mg, 0.40 mmol) and 4-methoxybenzaldehyde (110 mg, 0.81 mmol) following the general procedure for Knoevenagel condensation. The crude product was purified by recrystallization. Yield 186 mg (73 %); yellow solid; R_f = 0.4 (SiO_2; CH_2Cl_2); mp: 201 °C. ^{1}H NMR (500 MHz, $CDCl_3$) δ = 8.85–8.83 (m, 2H), 8.04 (d, ^{3}J = 16 Hz, 2H), 7.63–7.62 (m, 4H), 7.52–7.48 (m, 4H), 7.19 (s, 1H), 7.06 (d, ^{3}J = 16 Hz, 2H), 7.00–6.93 (m, 8H), 6.41–6.39 (m, 2H), 3.87 (s, 6H), 1.73 (s,

6H) ppm. ^{13}C NMR (125 MHz, $CDCl_3$) δ = 163.69, 163.45, 160.74, 143.27, 140.90, 138.60, 136.50, 131.49, 131.17, 130.07, 129.33, 128.80, 126.53, 125.40, 124.20, 120.70, 114.46, 114.33, 114.17, 55.52, 36.13, 31.51 ppm. HR-MALDI-MS (DCTB) m/z calcd for $C_{42}H_{34}N_3O_2$ [M-CH_3^+] 612.2646, found 612.2637.

(E,E)-2-[4-(9,9-Dimethyl-9,10-dihydroacridine)phenyl]-4,6-bis[(6-methoxynaphtalen-2-yl)ethenyl]pyrimidine (**4b**): Synthesized from compound **2** (100 mg, 0.26 mmol) and 6-methoxy-2-naphtalenaldehyde (96 mg, 0.51 mmol) following the general procedure for Knoevenagel condensation. The crude product was purified by recrystallization. Yield 133 mg (72 %); yellow solid; R_f = 0.3 (SiO_2; hexane/EtOAc 8:2); mp: 271 °C. ^{1}H NMR (500 MHz, $CDCl_3$) δ = 8.90–8.88 (m, 2H), 8.22 (d, ^3J = 16 Hz, 2H), 7.99 (s, 2H), 7.84–7.77 (m, 6H), 7.54–7.49 (m, 4H), 7.27–7.24 (m, 3H), 7.19–7.15 (m, 4H), 7.02–6.94 (m, 4H), 6.44–6.42 (m, 2H), 3.94 (S, 6H), 1.74 (s, 6H) ppm. ^{13}C NMR (125 MHz, $CDCl_3$) δ = 163.74, 163.39, 158.60, 143.35, 140.92, 138.54, 137.18, 135.29, 131.52, 131.42, 131.22, 130.12, 130.10, 129.04, 127.57, 126.56, 125.59, 125.43, 124.44, 120.73, 119.48, 114.58, 114.34, 106.10, 55.52, 36.15, 31.53 ppm. HR-MALDI-MS (DCTB) m/z calcd for $C_{50}H_{38}N_3O_2$ [M-CH_3^+] 712.2959, found 712.2944.

(E,E)-2-[4-(9,9-Dimethyl-9,10-dihydroacridine)phenyl]-4,6-bis[(4-diphenylaminophenyl)ethenyl]pyrimidine (**4c**): Synthesized from compound **2** (196 mg, 0.50 mmol) and 4-diphenylaminobenzaldehyde (274 mg, 1.00 mmol) following the general procedure for Knoevenagel condensation. The crude product was purified by column chromatography (hexane/CH_2Cl_2 1:1) and recrystallization. Yield 110 mg (22 %); yellow solid; R_f = 0.6 (SiO_2; hexane/CH_2Cl_2 1:1); mp: 233°C. ^{1}H NMR (500 MHz, $CDCl_3$) δ = 8.85–8.84 (m, 2H), 8.02 (d, ^3J = 16 Hz, 2H), 7.55–7.49 (m, 8H), 7.33–7.30 (m, 8H), 7.21–7.16 (m, 9H), 7.12–7.05 (m, 10H), 7.00–6.94 (m, 4H), 6.42–6.40 (m, 2H), 1.74 (s, 6H) ppm. ^{13}C NMR (125 MHz, $CDCl_3$) δ = 163.74, 163.44, 149.05, 147.81, 147.29, 143.25, 140.90, 138.66,

136.40, 131.49, 131.17, 130.07, 129.56, 129.47, 128.84, 126.52, 125.38, 125.26, 124.23, 123.93, 123.80, 122.51, 120.69, 114.34, 114.11, 36.13, 31.50 ppm. HR-MALDI-MS (DCTB) m/z calcd for $C_{64}H_{48}N_5$ [M-CH_3^+] 886.3904, found 886.3892.

Aknowledgements

M. F. Thanks the Région Bretagne, France, for founding her Ph D. F. B. and M.K. are indebted to the Ministry of Education, Youth and Sports of the Czech Republic (LTAIN19101).

References

[1] C. Adachi, *Jpn J. Appl. Phys.* **2014**, *53*, 60101.

[2] M. Y. Wong, E. Zysman-Colman, *Adv. Mater.*, **2017**, *29*, 1605444.

[3] M . N. Berberan-Santos, J. M. M. Garcia, *J. Am. Chem. Soc.*, **1996**, *118*, 9391-9394.

[4] I. S. Park, S. Y. Lee, C. Adachi, T. Yasuda, *Adv. Funct. Mater.*, **2016**, *26*, 1813-1821.

[5] a) Y. Tao, K. Yuan, T. Chen, P. Xu, H. Li, R. Chen, C. Zhang, L. Zhang, W. Huang, *Adv. Mater.*, **2014**, *26*, 7931-7958; b) T.-T. Biu, F. Goubard, M. Ibrahim-Ouadi, D. Gigmes, F. Dumur, *Appl. Sci.* **2018**, *8*, 494 ; c) H. Uoyama, K. Goushi, K. Shizu, H. Nomora, C. Adachi, *Nature*, **2012**, *492*, 234-238.

[6] P. K. Samanta, D. Kim, V. Coropceanu, J.-L. Brédas, *J. Am. Chem. Soc.*, **2017**, *139*, 4042-4051.

[7] F. Ma, G. Zhao, Y. Zheng, F. He, K. Hasrat, Z. Qi, *ACS Appl. Mater. Interfaces*, **2020**, *12*, 1179-1189.

[8] C.-Y. Chan, L.-S. Cui, J. U. Kim, H. Nakanotami, C. Adachi, *Adv. Funct. Mater.*, **2018**, 1706023.

[9] a) A. Tomkeviciene, T. Matulaitis, M. Guzauskas, V. Andruviciene, D. Volyniuk, J. V. Grazulevicius, *Org. Electron.*, **2019**, *70*, 227-239; b) M. Numata, T. Yasuda, C. Adachi, *Chem. Commun.*, **2015**, *51*, 9443-9446; c) C.-C. Tsai, W.-C. Huang, H.-Y. Chih, Y.-C. Hsh,

C.-W. Liao, C.-H. Lin, Y.-X. Kang, C.-H. Chang, Y. J. Chang, C.-W. Lu, *Org. Electron.*, **2018**, *63*, 166-174.

[10] I. S. Park, M. Nurmata, C. Adachi, T. Yasuda, *Bull. Chem. Soc. Jpn*, **2016**, *89*, 375-377.

[11] a) F. Baraket, B. Pedras, E. Torres, M. J. Brites, M. Dammak, M. N. Berberan-Santos, *Dyes Pigm.*, **2020**, *175*, 108114; b) Y. Liu, H. Huang, T. Zhou, K. Wu, M. Zhu, J. Yu, G. Xie, C. Yang, *J. Mater. Chem. C*, **2019**, *7*, 4778-4783; c) Y. Xiang, S. Gong, Y. Zhao, X. Yin, J. Luo, K. Wu, Z. Lu, C. Yang, *J. Mater. Chem. C*, **2016**, *4*, 9998-10004.

[12] a) J. W. Sun, J. Y. Baek, K. H. Kim, C. K. Moon, J.-H. Lee, S.-K. Kwon, Y.-H. Kim, J.-J. Kim, *Chem. Mater.*, **2015**, *27*, 6675-6681; b) J. W. Sun, J. Y. Baek, K.-H. Kim, J.-S. Huh, S.-K. Kwon, Y.-H. Kim, J.-J. Kim, *J. Mater. Chem. C*, **2017**, *5*, 1027-1032.

[13] a) F. Zheng, C. Wang, T. Meng, Y. Zhang, P. Zhang, Q. Shen, Y. Zhang, J. Zhang, J. Li, Q. Min, J. Chen, J.-J. Zhu, *ACS Nano* **2019**, *13*, 12577 – 12590; b) K.-Y. Pu, B. Liu, *Adv. Funct. Mater.* **2011**, *21*, 3408 – 3423; c) M. Deniβen, R. Hannen, D. Itskalov, L. Biesen, N. Nirmalananthan-Budau, K. Hoffmann, G. J. Reiss, U. Resch-Genger, T. J. J. Müller, *Chem. Commun.* **2020**, *56*, 7407-7410.

[14] a) Y. Yang, X. Yang, X. Fang, K. Z. Wang, D. Yan, *Adv. Sci.* **2018**, *5*, 1801187; b) E. Angioni, M. Chapran, K. Ivaniuk, N. Kostiv, V. Cherpak, P. Stakhira, A. Lazauskas, S. Tamulevičius, D. Volyniuk, N. J. Findlay, T. Tuttle, J. V. Grazulevicius, P. J. Skabara, *J. Mater. Chem. C* **2016**, *4*, 3851 – 3856; c) N. Nishimura, Z. Lin, K. Jinnai, R. Kabe, C. Adachi, *Adv. Funct. Mater.* **2020**, *30*, 2000795.

[15] a) K. Benelhadj, W. Muzuzu, J. Massue, P. Retailleau, A. Charaf-Eddin, A. D. Laurent, D. Jacquemin, G. Ulrich, R. Ziessel, *Chem. Eur. J.* **2014**, *20*, 12843-12857 ; b) V. S. Padalkar, S. Seki, *Chem. Soc. Rev.* **2016**, *45*, 169-202.

[16] a) Y. Geng, A. D'Aleo, K. Inada, L.-S. Cui, J. U. Kim, H. Nakanotami, C. Adachi, *Angew. Chem. Int. Ed.* **2017**, *129*, 16763-16767; b) M. Luo, X. Li, L. Ding, G. Baryshnikov, S. Shen,

M. Zhu, L. Zhou, M. Zhang, J. Lu, H. Ågren, X.-d. Wang, L. Zhu, *Angew. Chem. Int. Ed.* **2020**, *in press* doi : 10.1002/anie.202009077

[17] J. B. Birks, Photophysics of Aromatic Molecules, Wiley, London, 1970.

[18] a) J. Luo, Z. Xie, J. W. Y. Lam, L. Cheng, H. Chen, C. Qiu, H. S. Kwok, X. Zhan, Y. Liu, D. Zhu, B. Z. Tang, *Chem. Commun.*, **2001**, 1740-1741; b) Y. Chen, J. W. Y. Lam, R. T. K. Kwok, B. Liu, B. Z. Tang, *Mater. Horiz.*, **2019**, *6*, 428-433.

[19] a) S. Xiang, Z. Huang, S. Sun, X. Lv, L. Fan, S. Ye, H. Chen, R. Guo, L. Wang, *J. Mater. Chem. C*, **2018**, *6*, 11436-11443; b) J. Guo, Z. Zhao, B. Z. Tang, *Adv. Opt Mater.*, **2018**, *6*, 1800264; c) J. Zheng, J. Guo, H. Liu, J. W. Y. Lam, Z. Zhao, S. Chen, B. Z. Tang, *Chem. Asian J.*, **2019**, *14*, 828-835; d) M. R. Bryce, *Sci. China Chem.*, **2017**, *60*, 1561-1562; e) J. Wang, C. Liu, C. Jiang, C. Yao, M. Giu, W. Wang, *Org. Electron.*, **2019**, *35*, 170-178.

[20] a) S. Achelle, J. Rodriguez-López, F. Robin-le Guen, *ChemistrySelect*, **2018**, *3*, 1852-1886 ; b) K. Itami, D. Yamazaki, J.-i. Yoshida, *J. Am. Chem. Soc.*, **2004**, *126*, 15396-15397; c) S.-i. Kato, Y. Yamada, H. Hiyoshi, K. Umezu, Y. Nakamura, *J. Org. Chem.*, **2015**, *80*, 9076-9090.

[21] a) S. Achelle, I. Nouira, B. Pfaffinger, Y. Ramondenc, N. Plé, J. Rodríguez-López, *J. Org. Chem.*, **2009**, *74*, 3711-3717; b) S. Achelle, A. Barsella, C. Baudequin, B. Caro, F. Robin-le Guen, *J. Org. Chem.*, **2012**, *77*, 4087-4096; c) M. Fecková, P. le Poul, F. Robin-le Guen, T. Roisnel, O. Pytela, M. Klikar, F. Bureš, S. Achelle, *J. Org. Chem.*, **2018**, *83*, 11712-11726; d) F. Kournoutas, A. Fihey, J.-P. Malval, A. Spangenberg, M. Fecková, P. le Poul, C. Katan, F. Robin-le Guen, F. Bureš, S. Achelle, M. Fakis, *Phys Chem. Chem. Phys.*, **2020**, *22*, 4165-4176.

[22] a) S. Achelle, J. Rodríguez-López, F. Bureš, F. Robin-le Guen, *Chem. Rec.* **2020**, *20*, 440-451 ; b) S. Achelle, J. Rodríguez-López, N. Cabon, F. Robin-le Guen, *RSC Adv.*, **2015**, *5*, 107396-107399 ; c) S. Achelle, J. Rodríguez-López, C. Katan, F. Robin-le Guen, *J. Phys.*

Chem. C, **2016**, *120*, 26586-26995 ; d) S. Achelle, J. Rodríguez-López, M. Larbani, R. Plaza-Pedroche, F. Robin-le Guen, *Molecules*, **2019**, *24*, 1742.

[23] a) R. Komatsu, H. Sasabe, J. Kido, *J. Photonics Energy*, **2018**, ***8***, 032108; b) K. Nakao, H. Sasabe, R. Komatsu, Y. Hayasaka, T. Ohsawa, J. Kido, *Adv. Opt. Mater.*, **2017**, *5*, 1600843; c) R. Komatsu, H. Sasabe, K. Nakao, Y. Hayasaka, T. Ohsawa, J. Kido, *Adv. Opt. Mater.*, **2017**, *5*, 1600675; d) R. Komatsu, H. Sasabe, Y. Seino, K. Nakao, J. Kido, *J. Mater. Chem. C,* **2016**, *4*, 2274-2278; e) K. Wu, T. Zhang, L. Zhan, C. Zhong, S. Gong, N. Jiang, Z.-H. Lu, C. Yang, *Chem. Eur. J.*, **2016**, *22*, 10860-10866; f) I. S. Park, J. Lee, T. Yasuda, *J. Mater. Chem. C*, **2016**, *4*, 7911-7916; g) R. Komatsu, T. Ohsawa, H. Sasabe, K. Nakao, Y. Hayasaka, J. Kido, *ACS Appl. Mater. Interfaces*, **2017**, *9*, 4742-4749; h) T. Serevicius, R. Skaisgiris, J. Dodonova, L. Jagintavicius, D. Banevicius, K. Kazlauskas, S. Tunkevicius, S. Jursenas, *ACS Appl. Mater. Interfaces*, **2020**, *12*, 10727-10736; i) T. Serevicius, T. Baciunas, J. Bucevicius, J. Dodonova, S. Tunkevicius, K. Kazlauskas, S. Jursenas, *J. Mater. Chem. C*, **2018**, *6*, 11128-11136; j) P. Ganesan, R. Ranganathan, Y. Chi, X.-K. Liu, C.-S. Lee, S.-H. Liu, G.-H. Lee, T.-C. Lin, Y.-T. Chen, P.-T. Chou, *Chem. Eur. J.*, **2017**, ***23***, 2858-2866; k) J. S. Jang, H. L. Lee, K. H. Lee, J. Y. Lee*, J. Mater. Chem. C*, **2019**, *7*, 12695-12703.

[24] I. S. Park, H. Komiyama, T. Yasuda, *Chem. Sci.*, **2017**, *8*, 953-960.

[25] H. Yan, X. Meng, B. Li, S. Ge,Y. Lu, *J. Mater. Chem C*, 2017, **5**, 10589-10599.

[26] S. Achelle, Y. Ramondenc, F. Marsais, N. Plé, *Eur. J. Org. Chem.*, **2008**, 3129-3140.

[27] J.-J. Vanden Eynde, L. Pascal, Y. Van Haverbeke, P. Dubois, *Synth. Commun.*, **2001**, *31*, 3167-3173.

[28] C. Tang, Q. Zhang, D. Li, J. Zhang, P. Shi, S. Li, J. Wu, Y. Tian, *Dyes Pigm.*, **2013**, ***99***, 20-28.

[29] M. J. Frisch, G. W. Trucks, H. B. Schlegel, G. E. Scuseria, M. A. Robb, J. R. Cheeseman, G. Scalmani, V. Barone, G. A. Petersson, H. Nakatsuji, X. Li, M. Caricato, A. V. Marenich,

J. Bloino, B. G. Janesko, R. Gomperts, B. Mennucci, H. P. Hratchian, J. V. Ortiz, A. F. Izmaylov, J. L. Sonnenberg, D. Williams-Young, F. Ding, F. Lipparini, F. Egidi, J. Goings, B. Peng, A. Petrone, T. Henderson, D. Ranasinghe, V. G. Zakrzewski, J. Gao, N. Rega, G. Zheng, W. Liang, M. Hada, M. Ehara, K. Toyota, R. Fukuda, J. Hasegawa, M. Ishida, T. Nakajima, Y. Honda, O. Kitao, H. Nakai, T. Vreven, K. Throssell, J. A. Montgomery, Jr., J. E. Peralta, F. Ogliaro, M. J. Bearpark, J. J. Heyd, E. N. Brothers, K. N. Kudin, V. N. Staroverov, T. A. Keith, R. Kobayashi, J. Normand, K. Raghavachari, A. P. Rendell, J. C. Burant, S. S. Iyengar, J. Tomasi, M. Cossi, J. M. Millam, M. Klene, C. Adamo, R. Cammi, J. W. Ochterski, R. L. Martin, K. Morokuma, O. Farkas, J. B. Foresman, D. J. Fox, Gaussian 16, Revision A.03, **2016**.

[30] A. Ali, M. I. Rafiq, Z. Zhang, J. Cao, R. Geng, B. Zhou, W. Tang, *Phys. Chem. Chem. Phys.* **2020**, *22*, 7864-7874.

[31] F. Bureš, *RSC Adv.* **2014**, *4*, 58826–58851.

[32] M. Taniguchi, J. S. Lindsey, *Photochem. Photobiol.* **2018**, *94*, 290-327.

[33] a) R. Lartia, C. Allain, G. Bordeau, F. Schmidt, C. Fiorini-Debuisschert, F. Charra, M.-P. Teulade-Fichou, *J. Org. Chem.* **2008**, *73*, 1732-1744; b) C. Katan, M. Charlot, O. Mongin, C. Le Droumaguet, V. Jouikov, F. Terenziani, E. Badaeva, S. Tretiak, M. Blanchard-Desce, *J. Phys. Chem. B*, **2010**, *114*, 3152-3169.

[34] a) O. Bezvikonnyi, D. Gudeika, D. Volyniuk, V. Mimaite, B. Ronit Sebastine, J. V. Grazulevicius *J. Lumin.* **2019**, *206*, 250–259; b) J. Lee, K. Shizu, H. Tanaka, H. Nakanotani, T. Yasuda, H. Kaji, C. Adachi *J. Mater. Chem. C*, **2015**, *3*, 2175-2181.

[35] Y. Li, G. Xie, S. Gong, K. Wu, C. Yang, *Chem. Sci.*, **2016**, *7*, 5441-5447

[36] G. Xie, X. Li, D. Chen, Z. Wang, X. Cai, D. Chen, Y. Li, K. Liu, Y. Cao, S.-J. Su, *Adv. Mater.* **2016**, *28*, 181-187.

[37] G. M. Sheldrick, *Acta Cryst.*, **2015**, *A71*, 3-8

10.1002/chem.202004328

[38] G. M. Sheldrick, *Acta Cryst.*, 2015, **C71**, 3-8